A Novel Method for InSAR Phase Unwrapping with Single Baseline

Chenxi Tian and Guoman Huang
Chinese Academy of Surveying and Mapping, Haidian District, Beijing, China

Keywords: Interferometric Synthetic Aperture Radar (InSAR), Single-Baseline (SB), Multi-Baseline (MB), Phase Unwrapping (PU).

Abstract: The precision of phase unwrapping (PU), one of the primary methods used in interferometric synthetic aperture radar (InSAR), has a direct impact on the accuracy of the digital elevation model (DEM) that InSAR produces. The phase continuity assumption restricts single-baseline (SB) PU, and it is frequently hard to achieve optimal PU results in complex terrain areas with significant gradient variations. Fortunately, by utilizing numerous InSAR interferograms, or the elevation changes corresponding to each interference fringe in the interferogram, multi-baseline (MB) PU can totally overcome the restriction of the phase continuity assumption. Therefore, this paper proposes a virtual-baseline (VB) PU based on the two-stage programming (TSPA) MB PU approach to transform the SB PU problem into a MB PU problem. The novel method can be referred to as VB-TSPA. First, the effect of baseline length on MB PU is comprehensively considered to determine the virtual baseline length. Then a corresponding interferogram is simulated according to the length. Finally, the TSPA method is used for the MB PU. The experimental results from simulated and real data demonstrate that the novel PU method has a better effect than the traditional SB PU algorithm and can obtain higher precision DEM.

1 INTRODUCTION

Interferometric synthetic aperture radar (InSAR) is a technique for tracking ground deformation even in inclement weather or at night. It has been widely used in building digital elevation model (DEM) for topographic mapping and extracting deformation fields for surface deformation monitoring (Wang, Ch, Zhang, H, & Liu, Z, 2002). InSAR technology can retrieve terrain elevation information through phase (Liao, M & Lin, H, 2003). However, the temporal and spatial decoherence contribute to generating the phase noise easily. Phase undersampling and spectrum aliasing are major issues that have a direct impact on the accuracy, solvability, and reliability of elevation information inversion in complicated terrain areas, such as those with steep slopes and discontinuities (Jin, G, Zhang, H, & Xu, Q, 2015). Phase unwrapping (PU) is one of the key steps of InSAR, and its precision directly affects the accuracy of the DEM generated by InSAR.

At present, single-baseline (SB) PU methods can be divided into three categories: path-following methods, optimization-based methods, integrated denoising and unwrapping methods. Path-following algorithms mainly include branch-cut method (Goldstein, R, Zebker, H, & Werner, C, 1988), quality-guided method (Anand, A & Zhou, W, 1988; Zhong, H & Li, H, 2021), etc. Generally, the path-following methods have high efficiency when the interferograms with high signal-noise ratio. Yet, when processing interferograms with low quality, the methods result in unwrapping failure. The minimum cost flow (MCF) algorithm (Costantini, M, 1988), a typical example of the optimization-based methods, transforms the PU problem into the network cost minimization problem, which can obtain relatively robust PU results from the interferogram with litle noise. There are also some methods, such as weighting least square method (Ghiglia, D & Romero, L, 1994) and the least squares based on the fast Fourier transform method (Pritt, M. & Shipman, J, 1994) that can unwrap continuously and smoothly. Unfortunately, the dynamic range of unwrapping phase is quickly reduced, resulting in serious distortion of fringe details. Integrated denoising and unwrapping methods include extended Kalman filtering PU algorithm (Estahbanati, A. & Dehghani, M, 2018), unscented Kalman filtering PU algorithm (XIE, X., 2016), can retrieve ideal unwrapping results

Tian, C. and Huang, G.
A Novel Method for InSAR Phase Unwrapping with Single Baseline.
DOI: 10.5220/0011839300003473
In *Proceedings of the 9th International Conference on Geographical Information Systems Theory, Applications and Management (GISTAM 2023)*, pages 60-68
ISBN: 978-989-758-649-1; ISSN: 2184-500X

taking long time. Moreover, the deep learning algorithm has also been applied to the field of PU (Sica, F, Calvanese, F, & Scarpa, G, 2020; Ferraioli, G., 2021), and excellent unwrapping results have been obtained in some examples. These methods are conducive to expanding the application field of PU technology.

The majority of the SB PU methods mentioned above rely on the assumption of phase continuity, which necessitates that the observation region have enough spatial continuity. Sadly, the prerequisites of this hypothesis cannot be met by valleys, steep peaks, cliffs, and other complex terrain, which frequently prevents the optimum PU results. The multi-baseline (MB) InSAR technology performs microwave imaging in the same area under different baseline conditions, resulting in the formation of multiple interferograms (Yu, H., Lan, Y., & Yuan, Z., 2019). It can effectively overcome or reduce the adverse effects caused by the surge of target height, large noise interference and other factors, so that it has the potential to access high precision DEM in the reconstruction of discontinuous terrain elevation. The MB PU method can be divided into two main categories : parameter-based methods and non-parameter-based methods. The first set of methods adopt InSAR probability density functions to construct a statistical framework, using maximum likelihood (ML) or maximum a posteriori (MAP) criteria to estimate PU results (Pascazio & Schirinzi,G, 2000; Fornaro,G, Monti, G., Pauciullo, A, & DeZan, F, 2006). The method of the second group transformed MB PU problem into an unsupervised learning problem; then, cluster analysis (CA) is used to estimate the unentanglement results group by group (Jiang, J, Wang, Q, & Zhou, Z, 2017). It is worth noting that the two-stage programming (TSPA) method (Yu, H. & Lan, Y, 2016) establishes the connection between SB PU and MB PU. In the first stage, TSPA estimates the difference in ambiguity number between adjacent pixels using interferograms of different baseline lengths based on the formulation of the Chinese remainder theorem (CRT). In the second stage, the SB PU methods are used to calculate the MB residues.

In order to obtain reliable PU results for complex terrain in the instance of the SB InSAR system, this study suggests a virtual-baseline (VB) PU based on the two-stage programming MB PU approach (TSPA), referred to as VB-TSPA. By comprehensively considering the impact of baseline length on the PU performance of multiple baselines, an appropriate virtual baseline length is selected. Afterwards, a simulated interferogram with the baseline length is created. The double-baseline (DB) PU is employed with the TSPA approach as a last step. In order to get over the restriction of the phase continuity assumption and determine the true phase of complicated terrain, the SB PU problem is turned into the MB PU problem in this paper. The approach is capable of successfully addressing the PU problem of complex terrain, according to experimental results.

2 VB-TSPA PU METHOD

2.1 SB PU Converts to DB PU

The primary goal of PU is to choose a pixel in the interferogram as a reference point in order to recover the true phase of the other pixels (relative to the reference point) from the wrapped interferogram (that is, the phase of the interferogram range cycling between -π and π). As follows:

$$\Psi(s) = \varphi(s) + 2k(s)\pi \tag{1}$$

where $\Psi(s)$ is the absolute phase of the sth pixel, $\varphi(s)$ is the wrapped phase of the sth pixel and $k(s)$ is called the ambiguity number of the sth pixel (Gao, Y., Tang, X., & Li, T., 2022).

It can be seen from equation (1) that SB PU is an ill-posed inverse problem, hence, almost all SB PU methods make a hypothesis, namely phase continuity assumption, to overcome this problem. However, system noise and sudden terrain changes often lead to the failure of the hypothesis in practical applications. Promisingly, MB PU can significantly increase the fuzzy interval of the interference phase by using the diversity of the baseline, which completely overcomes the limitation of the phase continuity assumption. The VB-TSPA PU method is described in detail below.

For the InSAR system, the relation between the terrain height and the absolute phase is

$$h(s) = \frac{\lambda \cdot R(s) \cdot sin(\theta)}{B \cdot 4\pi} \cdot \Psi(s) \tag{2}$$

where $h(s)$ is the terrain height of the sth pixel, λ is the wavelength, $R(s)$ is the slant range of the target from the master channel of the sth pixel, θ is the incidence angle, and B is the vertical baseline (referred to as baseline) (Baselice, F, Ferraioli, G, Pascazio, V, & Schirinzi, G, 2014; Liu, H, Xing, M, & Bao, Z, 2015).

Then, the VB length B_2 is selected to form the optimal baseline combination with the baseline length B_1 of the original interferogram. After simulating an

interferogram with the length of B_2, we can link the true phase of the two interferograms by combining (1) and (2):

$$B_2(\varphi_1(s) + 2k_1(s)\pi) = B_1(\varphi_2(s) + 2k_2(s)\pi) \quad (3)$$

where $k_1(s)$ and $k_2(s)$ are the ambiguity numbers of the sth pixel in original interferogram and simulated interferogram, respectively. $\varphi_1(s)$and $\varphi_2(s)$ are the wrapped phase of the sth pixel in the original interferogram and simulated interferogram, respectively.

If choosing a neighboring pixel s-1 of pixel s, from (3), and letting (3) subtract it, we will get

$$B_2((\varphi_1(s) - \varphi_1(s-1)) + 2(k_1(s) - k_1(s-1)\pi)) = B_2((\varphi_1(s) - \varphi_1(s-1)) + 2(k_1(s) - k_1(s-1)\pi)) \quad (4)$$

If we let $k_1(s) - k_1(s-1) = \hat{\Delta}k_1(s, s-1)$ and $k_2(s) - k_2(s-1) = \hat{\Delta}k_2(s, s-1)$, (4) will become

$$B_2((\varphi_1(s) - \varphi_1(s-1)) + 2\hat{\Delta}k_1(s, s-1)\pi)) = B_2((\varphi_1(s) - \varphi_1(s-1)) + 2(\hat{\Delta}k_2(s, s-1)\pi)) \quad (5)$$

Using the CRT method, $\hat{\Delta}k_1(s, s-1)$ and $\hat{\Delta}k_2(s, s-1)$ can be obtained as new gradient information between adjacent pixels of two interferograms, respectively. Next, the MCF method is adopted to solve the DB PU residues.

2.2 Principle of VB Length Selection

The VB-TSPA PU method is a subset of DB PU methods, and any combination of baselines of the problem can be solved by using the CRT. Nevertheless, the CRT are sensitive to baseline length. Even if the same PU method is chosen, varied baseline lengths will result in different PU performance. Obviously, the SB PU problem is unable to transform from ill-posed to well-posed by simply increasing the number of interferograms without any restriction on the baseline length.

Yu, H., Lee, H., Cao, N., & Lan, Y (2019), proposed a nonlinear mixed-integer programming-based baseline design criterion (referred to NIP criterion) to maximize the MB PU's CRT-based measurement deviation tolerance.

$$B_2(\varphi_1(s) + n_1(s) + 2k_1(s)\pi) = B_1(\varphi_2(s) + n_2(s) + 2k_2(s)\pi) \quad (6)$$

Where $n_i(s)(i = 1,2)$represents the general system observation noise of the sth pixel in the interferogram i.

$$\begin{aligned} arg \min_{k_1(s),k_2(s)} |B_2(\varphi_1(s) + n_1(s) + 2k_1(s)\pi) \\ - B_1(\varphi_2(s) + n_2(s) \\ + 2k_2(s)\pi)| \\ r^L_{k_1(s)} \le k_1(s) \le r^U_{k_1(s)} \\ r^L_{k_2(s)} \le k_2(s) \le r^U_{k_2(s)} \\ k_1(s), k_2(s) \in integer \end{aligned} \quad (7)$$

where $k_1(s)$ and $k_2(s)$ are the decision variables, ($r^L_{k_1(s)}$, $r^U_{k_1(s)}$) and ($r^L_{k_2(s)}$, $r^U_{k_2(s)}$) are the CRT searching windows of $k_1(s)$and $k_2(s)$, respectively.

$$W_i = r^L_{k_i(s)} + r^U_{k_i(s)} (i = 1, 2) \quad (8)$$

According to the NIP requirement, CRT prefers MB InSAR baseline lengths that increase correspondingly as the size of the available CRT searching windows increases. Only the length of the CRT search window in the long baseline is relevant to the OPT requirement of the NIP criterion. When $\frac{B_2}{B_1} \ge W_2 + 1$, the results of MB PU are optimal. Where B_2 is the long baseline, B_1 is the short baseline, and W_2 is the CRT search window size of the long baseline (Yu, H., Lee, H., Cao, N., & Lan, Y, 2019).

The size of the search window can be estimated by using some prior knowledge, such as rough terrain information (Yu, H., Lee, H., & Cao, N., 2018). If the terrain changes greatly, the search window should also be large. In addition, the search window W_2 corresponding to the long baseline can be estimated by the following formula:

$$W_2 = 2 \cdot \text{round}\left(\frac{g_{max} \cdot \alpha \cdot B_c}{\lambda \cdot R \cdot sin(\theta)}\right) (0<\alpha\le 1) \quad (9)$$

where α is a scaling factor and in some systems, is believed to be 0.1(Moreira, A., Prats-Iraola, P., & Younis, M., 2013). $g_{max}$is the maximum gradient (i.e. the maximum height difference between adjacent pixels) in the observation area. B_c is known as the critical baseline for which the two SAR images become completely decorrelated.

Additionally, in order to reduce the PU error sensitivity of MB InSAR system, the longer B_i (i = 1, 2), the better the performance. Also, the increase of B_i (i = 1, 2) can minimize the impact of baseline error on DEM accuracy (Yu, H., Xing, M., & Yuan, Z, 2021). Summarily, appropriate baseline length should be chosen comprehensively to achieve the best performance.

3 EXPERIMENTAL RESULTS

In order to confirm the viability of the suggested method, the performance of the VB-TSPA PU method was tested on simulated data and real data, respectively, and compared to the conventional SB PU method. As one of the most widely used SB PU methods at present, the MCF PU method has advantages in operation time and PU precision, which can improve the computational efficiency. Moreover, the algorithm can limit the error to a small range, prevent the error transmission, and the PU result is more accurate. Consequently, the MCF PU method is chosen in this paper for comparison.

3.1 Simulated Data

Fig. 1 is a 3D view of the simulated mountain terrain with a size of 256 ×256 pixels and an elevation range of 0-700 meters. Fig. 2 is the interferogram corresponding to the terrain in Fig. 1 obtained by simulating the system parameters in Table 1. Fig. 2(a) and (b) show the reference unwrapping phase and the wrapping phase containing noise, with the baseline length of 700 meters, respectively. Meanwhile, Fig. 2(b) is also the interferogram to be unwrapped. Fig. 2(c) is a noiseless wrapping phase with a baseline length of 100 meters determined according to the baseline length selection principle of the VB-TSPA method.

Fig. 3 and Fig. 4 are the results obtained by using the MCF and VB-TSPA methods to unwrap Fig. 2(b), respectively. From Fig. 3(a), we can clearly see discontinuous terrain changes (marked by rectangular boxes), while Fig. 4(a) has continuous phase changes. From a visual interpretation perspective, the method presented in this paper yields a better unwrapping result. For further quantitative evaluation of the performance, the normalized root-mean-square error (NMSE) of the PU accuracy is defined as:

$$\xi = \sqrt{\frac{\left\| \widehat{\phi} - \phi \right\|^2}{\left\| \phi \right\|^2}} \tag{10}$$

where ϕ is the vector collecting from the reference unwrapped phase, $\widehat{\phi}$ is the vector collecting from the estimated unwrapped phase, and $\| \ \|^2$ is the quadratic norm. The smaller the ξ is, the higher the unwrapping precision is generated and the better the unwrapping result is achieved. Therefore, it can be seen from Table 2 that the NMSE of the unwrapping result of the VB-TSPA method is lower than that of the MCF method, and the error range is also narrower, confirming the method's efficacy.

Table 1: Major parameters of simulated InSAR system.

Orbit Altitude	Incidence Angle	Wavelength
785km	19°	5.7cm

Table 2: Evaluation results of the simulation data set.

PU method	NMSE	Error range(rad)
MCF	0.1312	[-9.3,6.2]
VB-TSPA	0.0156	[-3.1,3.1]

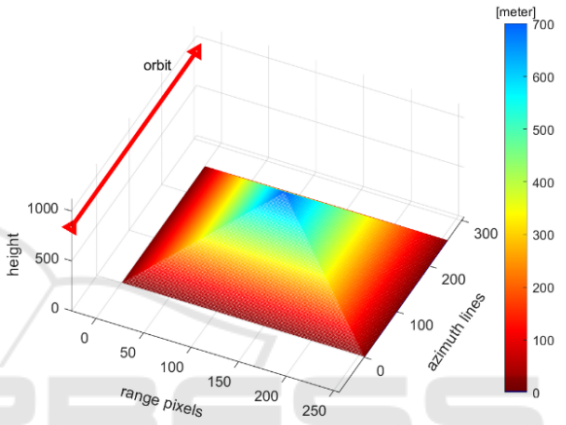

Figure 1: Reference terrain height.

3.2 China-TH2 InSAR Data

In the real data experiment of this study, the data is by the China_TH2 system, and its main parameters are shown in Table 3. The amplitude image of the experiment area, shown in Fig. 5, reveals that the region is geographically distinguished by a significant amount of mountainous and rough terrain. In this situation, the phase continuity assumption may not be effective, making it challenging to achieve correct results for SB PU methods. Fig. 6 depicts the simulated unwrapped phase of the region after removing the flat-earth phases.

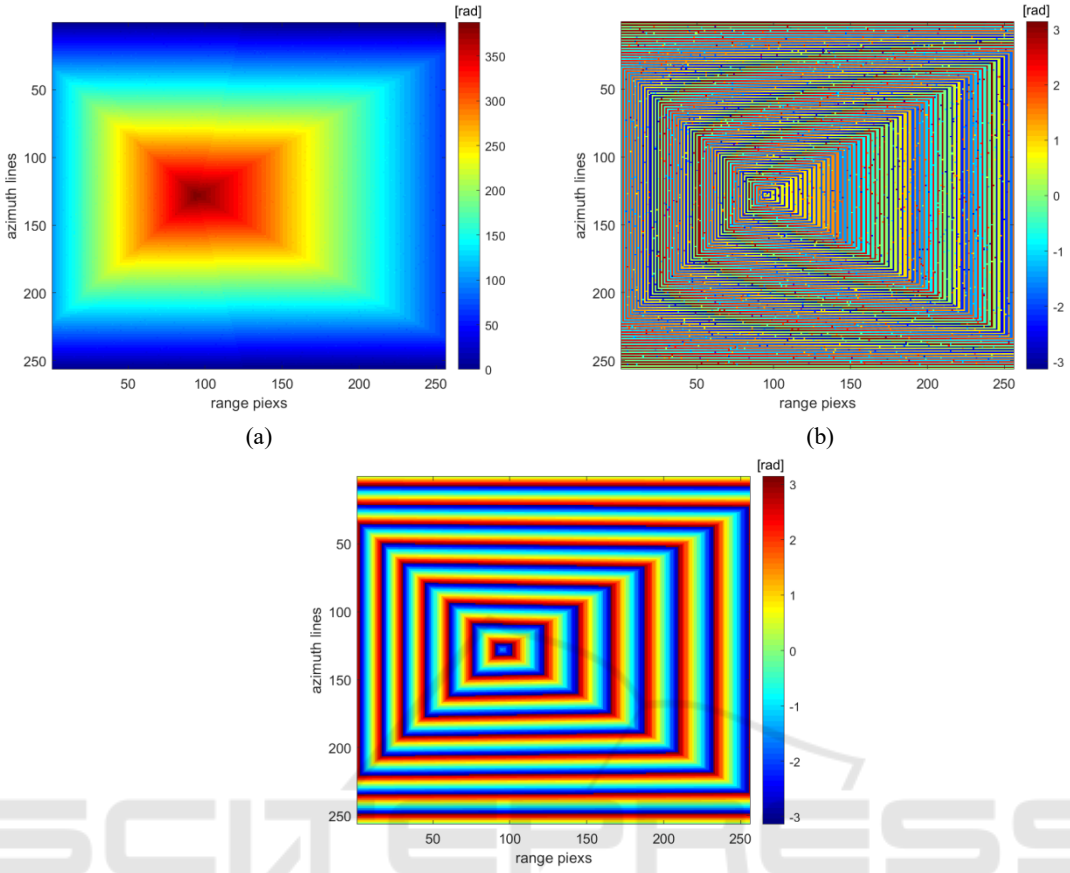

Figure 2: Simulated interferograms: (a) reference unwrapped phases with long baseline; (b) simulated noise-containing wrapped phases with long baseline; (c) simulated noise-free wrapped phases with short baseline.

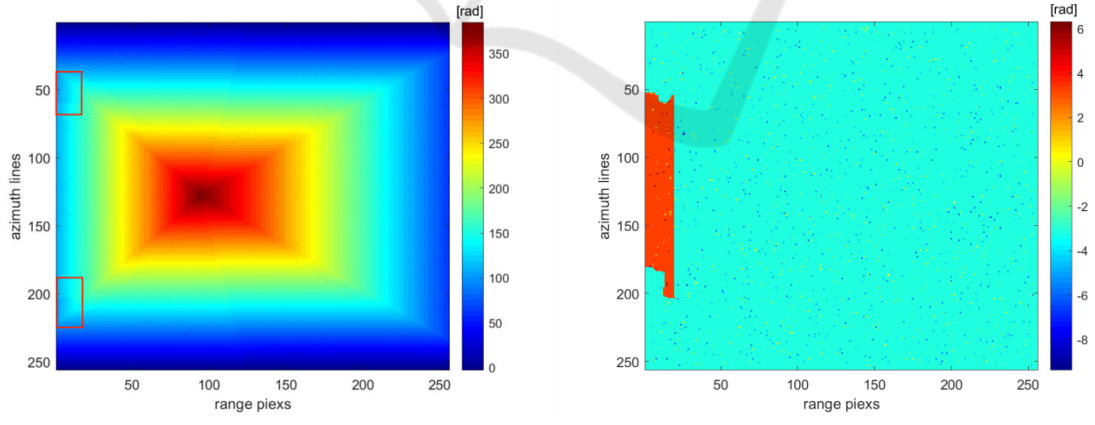

Figure 3: PU results of Fig. 2(b) obtained by MCF: (a) unwrapped phases; (b) errors between (a) and Fig.2(a).

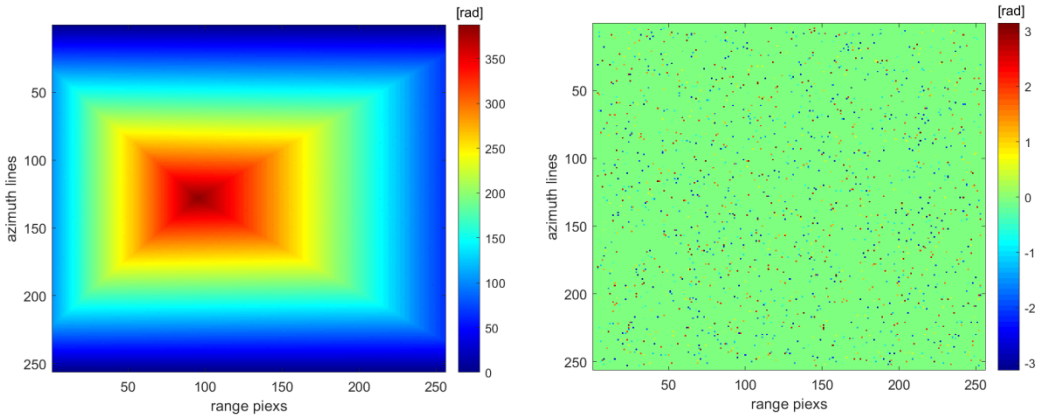

(a) (b)

Figure 4: PU results of Fig. 2(b) obtained by VB-TSPA: (a) unwrapped phases; (b) errors between (a) and Fig.2(a).

Fig. 7 is the coherence coefficient of the data, whose interferometric coherence coefficient is 0.38. The low coherent images limit the accuracy of the interferometric phase measurement. Fig. 8 is the flattened interferogram and its local magnification obtained from the real data. Meanwhile, it is the interferogram to be unwrapped. Next, the MCF method and the VB-TSPA method will be used for PU of Fig. 8(a). According to the principle of virtual baseline length selection, the length in this experiment is 83.8780 meters, and the simulated interferogram is displayed in Fig. 9(a).

Fig. 10 and Fig. 11 show the PU results accessed by the MCF and VB-TSPA method, respectively. It can be seen from the figures that the interference pattern fringe details got by the MCF method are seriously distorted, while the unwrapping result obtained by the VB-TSPA method is similar to the reference unwrapping result. The error range is substantially narrower than that of the MCF approach, and the NMSE of the PU result acquired by the VB-TSPA method is much closer to 0. For long baseline interferogram and rapid phase change in complex terrain, the VB-TSPA PU method displays better performance than the MCF PU method. Evidently, it can be concluded that the VB-TSPA method suggested in this paper is more accurate and reliable.

The DEM of this region was created by an elevation inversion of the unwrapping phase achieved by the VB-TSPA method, as shown in Fig. 12. Additionally, the accuracy of the DEM inversion produced by the PU solution was further assessed using 221 control points taken from an external DEM, and the final median error was 22.45m. Apparently, the VB-TSPA method can produce high precision DEM.

4 CONCLUSIONS

The VB-TSPA PU proposed in this study transforms the SB PU problem into the MB PU problem, breaks through the limitation of phase continuity assumption, and can obtain the unwrapped phase of complicated terrain in the case of SB InSAR system. The efficiency of the VB-TSPA PU algorithm has been demonstrated by experimental findings using real and simulated data. Compared with the MCF PU method, it can achieve more accurate results under the conditions of dense interference fringes and complex terrain, and produce high-precision DEM of the region. Although the influence of noise on the PU results is reduced by global optimization in this paper, there is still room for improving the robustness of this method as the mathematical basis of the method is CRT.

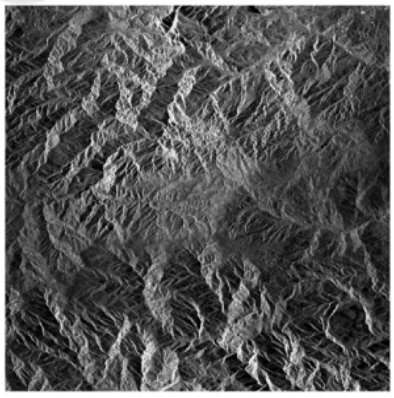

Figure 5: Amplitude image.

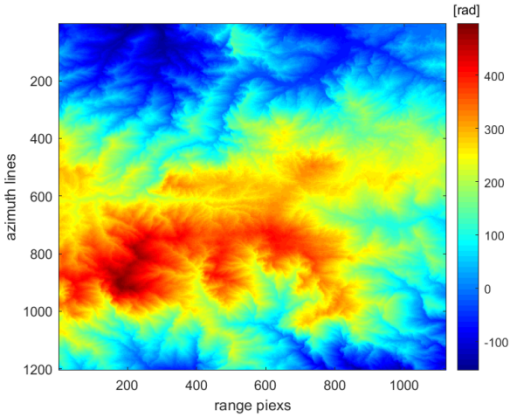

Figure 6: Simulated unwrapped phase (flattened).

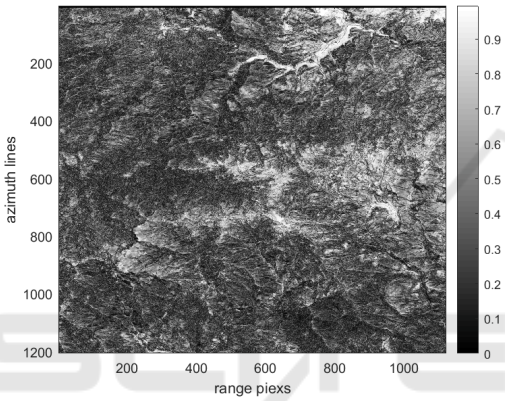

Figure 7: Coherence image.

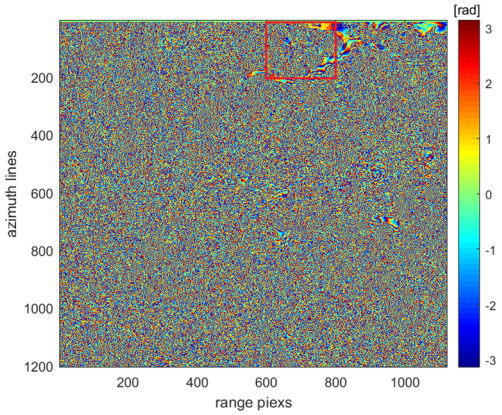

(a) Wrapped phases (flattened).

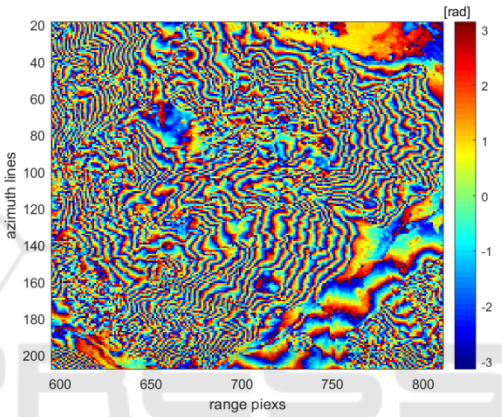

(b) Marked by rectangular boxes in (a).

Figure 8: Interferogram of China-TH2 data set.

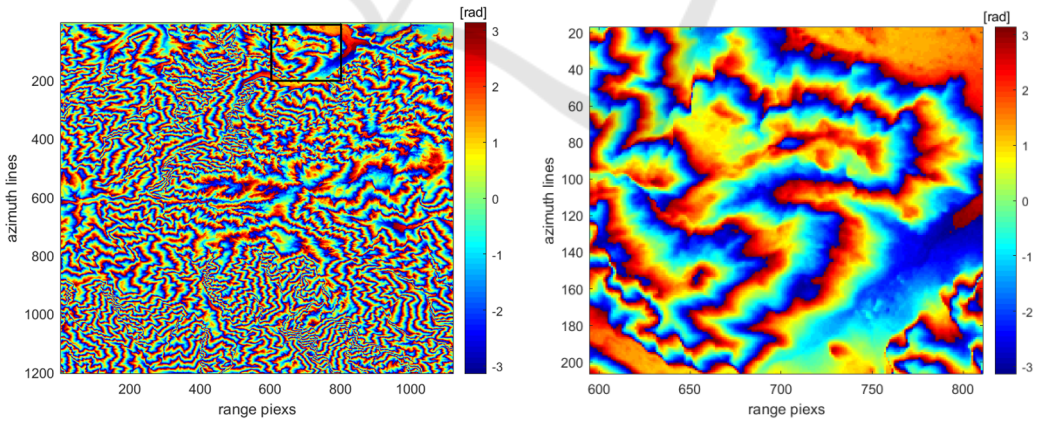

(a) (b)

Figure 9: Simulated Interferogram: (a) Wrapped phases (flattened); (b) Marked by rectangular boxes in (a).

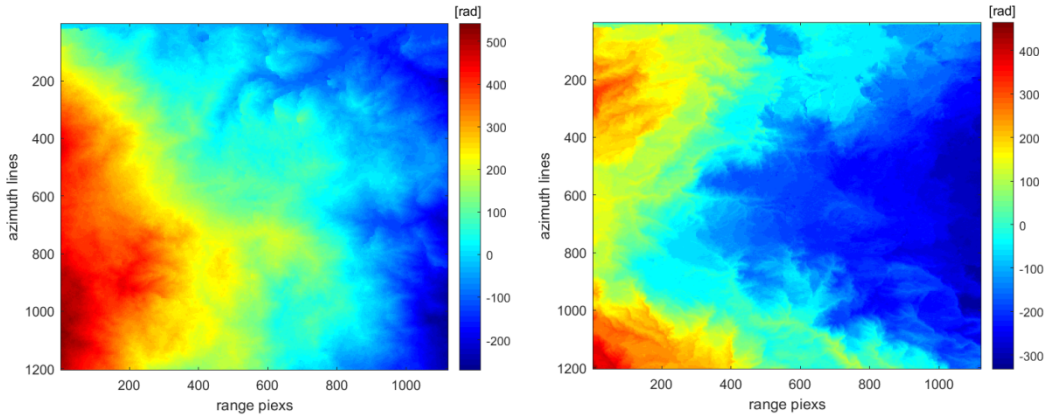

(a) (b)

Figure 10: PU results of Fig. 8(a) obtained by MCF: (a) unwrapped phases (flattened) ; (b) errors between (a) and Fig. 8(a).

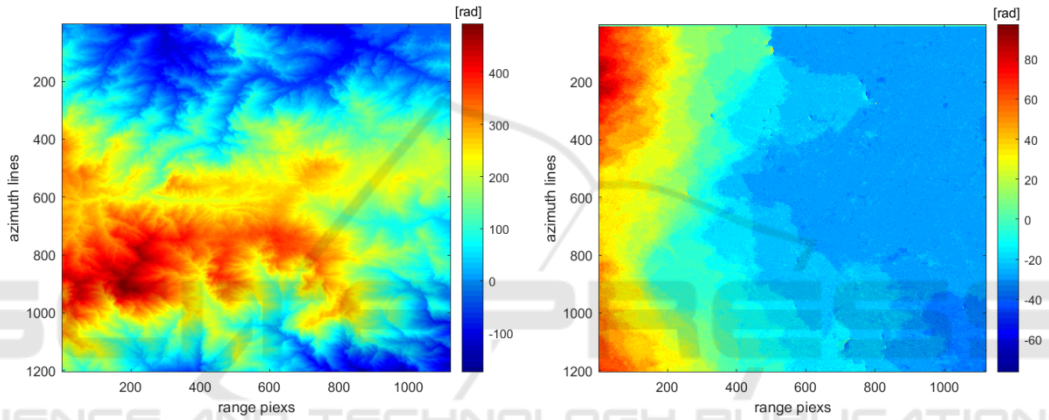

(a) (b)

Figure 11: PU results of Fig. 8(a) obtained by VB-TSPA: (a) unwrapped phases (flattened); (b) errors between (a) and Fig. 8(a).

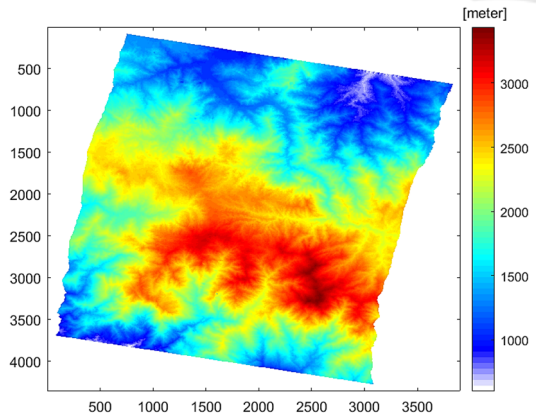

Figure 12: Terrain height estimated by the PU solution of the VB-TSPA method.

Table 3: Major parameters of China-TH2 InSAR system.

Orbit Altitude	517.597km
Wavelength	3.12cm
Latitude	9.65°
longitude	-83.80°
Incidence Angle	41.19°
Normal Baseline	587.1457m

Table 4: Evaluation results of the China-TH2 data set.

PU method	NMSE	Error range (rad)
MCF	0.8677	[-332.8,464.8]
VB-TSPA	0.3617	[-76.4,97.3]

ACKNOWLEDGEMENTS

This work was supported in part by National Key Research and Development project (2022YFB3901604) and CSAM FUNDING : 3D

information construction of array SAR point cloud research (AR2206).

REFERENCE

Anand, A, & Zhou, W. (1988). Fast phase-unwrapping algorithm based on a gray-scal mask and flood fill. Applied optics, 37(23): 5416-5420.

Baselice, F, Ferraioli, G, Pascazio, V, & Schirinzi, G. (2014). Contextual information-based multichannel synthetic aperture radar interferometry: Addressing DEM reconstruction using contextual information. IEEE Signal Process. Mag, vol. 31, no. 4, pp. 59‑68.

Costantini, M. (1988). A novel phase unwrapping method based on network programming. *IEEE Trans. Geosci. Remote Sense*, 813–821.

Estahbanati, A., & Dehghani, M. (2018). A Phase Unwrapping Approach Based on Extended Kalman Filter for Subsidence Monitoring Using Persistent Scatterer Time Series Interferometry. IEEE Journal of Selected Topics in Applied Earth Observations and Remote Sensing, vol. 11, no. 8, pp. 2814-2820, Aug.

Ferraioli, G. (2021). Joint Phase Unwrapping and Speckle Filtering by Using Convolutional Neural Networks. *IEEE International Geoscience and Remote Sensing Symposium IGARSS, 2021*, (pp. 3376-3379).

Fornaro,G, Monti, G., Pauciullo, A, & DeZan, F. (2006). Maximum likelihood multi-baseline SAR interferometry. Proc. Inst. Electr. Eng., vol. 153, no. 3, pp. 279‑288.

Gao, Y., Tang, X., & Li, T. (2022). A Phase Slicing 2-D Phase Unwrapping Method Using the L 1 -Norm. IEEE Geoscience and Remote Sensing Letters, 19, 1‑5.

Ghiglia, D, & Romero, L. (1994). Robust two-dimensional weighted and unweighted phase unwrapping that uses fast transforms and interative methods. Journal of the optical society of America, 11(1): 107-117.

Goldstein, R, Zebker, H, & Werner, C. (1988). Satellite radar interferometry: two-dimensional phase unwrapping. Radio science, 23(4): 713-720.

Jiang, J, Wang, Q, & Zhou, Z. (2017). A refined clusteranalysis-based multibaseline phase-unwrapping algorithm. IEEE Geosci. Remote Sens. Lett., vol. 14, no. 9, pp. 1565‑1569.

Jin, G, Zhang, H, & Xu, Q. (2015). Radar photogrammetry. Beijing: Surveying and Mapping Press.

Liao, M, & Lin, H. (2003). Synthetic aperture radar interferometry: principle and signal processing. Beijing: Surveying and Mapping Press.

Liu, H, Xing, M, & Bao, Z. (2015). A cluster-analysis-based noise-robust phase-unwrapping algorithm for multibaseline interferograms. EEE Trans. Geosci. Remote Sens., vol. 53, no. 1, pp. 494‑504.

Moreira, A., Prats-Iraola, P., & Younis, M. (2013). A tutorial on synthetic aperture radar. IEEE Geoscience and Remote Sensing Magazine, 1(1), 6‑43.

Pascazio, & Schirinzi,G. (2000). Multifrequency InSAR height reconstruction through maximum likelihood estimation of local planes parameters. IEEE Trans. Image Process, vol. 11, no. 12, pp. 1478‑1489.

Pritt, M., & Shipman, J. (1994). Least-squares two-dimensional phase unwrapping using FFT's. IEEE Transactions on Geoscience and Remote Sensing.

Sica, F, Calvanese, F, & Scarpa, G. (2020). A CNN-Based Coherence-Driven Approach for InSAR Phase Unwrapping. IEEE Geoscience and Remote Sensing Letters, 99.

Wang, Ch, Zhang, H, & Liu, Z. (2002). Space borne synthetic aperture radar interferomet. Bejing: Science press.

XIE, X. (2016). Iterated unscented Kalman filter for phase unwrapping of interferometric fringes. Optics Express, 24(17): 18872-18897.

Yu, H., Lee, H., & Cao, N. (2018). A novel method for deformation estimation based on multibaseline InSAR phase unwrapping. IEEE Trans. Geosci. Remote Sens., vol. 56, no. 9, pp. 5231‑5243.

Yu, H., & Lan, Y. (2016). Robust Two-Dimensional Phase Unwrapping for Multibaseline SAR Interferograms: A Two-Stage Programming Approach. IEEE Transactions on Geoscience and Remote Sensing, 54(9), 5217‑5225.

Yu, H., Lan, Y., & Yuan, Z. (2019). Phase Unwrapping in InSAR: A Review. IEEE Geoscience and Remote Sensing Magazine, 7(1), 40‑58.

Yu, H., Lee, H., Cao, N., & Lan, Y. (2019). Optimal Baseline Design for Multibaseline InSAR Phase Unwrapping. IEEE Transactions on Geoscience and Remote Sensing, 57(8), 5738‑5750.

Yu, H., Xing, M., & Yuan, Z. (2021). Baseline Design for Multibaseline InSAR System: A Review. IEEE Journal on Miniaturization for Air and Space Systems, 2(1), 17‑24.

Zhong, H, & Li, H. (2021). Path-following Phase Unwrapping Algorithm based on Priority-guided Map. *2021 14th International Congress on Image and Signal Processing, BioMedical Engineering and Informatics (CISP-BMEI)*, (pp. 1-6).